

# Path integration of head direction: updating a packet of neural activity at the correct speed using neuronal time constants

D. M. Walters · S. M. Stringer

Received: 6 July 2009 / Accepted: 27 November 2009 / Published online: 26 May 2010  
© Springer-Verlag 2010

**Abstract** A key question in understanding the neural basis of path integration is how individual, spatially responsive, neurons may self-organize into networks that can, through learning, integrate velocity signals to update a continuous representation of location within an environment. It is of maximal importance that this internal representation of position is updated at the correct speed, and in real time, to accurately reflect the motion of the animal. In this article, we present a biologically plausible model of velocity path integration of head direction that can solve this problem using neuronal time constants to effect natural time delays, over which associations can be learned through associative Hebbian learning rules. The model comprises a linked continuous attractor network and competitive network. In simulation, we show that the same model is able to learn two different speeds of rotation when implemented with two different values for the time constant, and without the need to alter any other model parameters. The proposed model could be extended to path integration of place in the environment, and path integration of spatial view.

**Keywords** Path integration · Head direction cells · Continuous attractor network · Competitive network · Neuronal time constant

A key problem to be addressed is how, through learning, these cells may self-organize to form networks that can perform the necessary calculations for spatial navigation. In this article, we consider the process of path integration, where an animal integrates idiothetic (self-motion) cues, such as forward motion or rotation, to update its internal representation of its position or orientation within an environment (Mittelstaedt and Mittelstaedt 1980, 1982; Collett and Zeil 1998; Redish 1999).

It has been shown in previous research that when presented with a continuous input space, a layer of recurrently connected neurons can form a continuous attractor network. Within this network, a local packet of persistent activity (a stable state) can represent a particular directional heading or location (Amari 1977; Taylor 1999). A continuous attractor can support a continuous space of stable memory states, and can, thus, learn to represent any given location or directional

D. M. Walters (✉) · S. M. Stringer  
Department of Experimental Psychology, Oxford Centre  
for Theoretical Neuroscience and Artificial Intelligence,  
South Parks Road, Oxford OX1 3UD, UK  
e-mail: daniel.walters@psy.ox.ac.uk  
URL: www.oftnai.org

heading. With training on a continuous sensory space, such as location or head direction, after associative Hebbian learning, the strength of the synapses between any two neurons will be a function of the degree of overlap of their receptive fields (the larger the overlap, the stronger the synapse) and, thus, symmetric. Thus, the strengths of the synapses between any given individual neuron and all other neurons in the network are described by an approximately Gaussian distribution, with the synaptic strengths again determined by the degree of receptive-field overlap. This symmetry ensures that a packet of neural activity representing a directional heading or a location can remain stable (unlikely to drift) and persist within the continuous attractor network when the animal is not moving.

An asymmetric external input is required to drive the activity packet around the continuous attractor network and, thus, update the location of the activity packet in the attractor space. In this manner, the activity packet will track the exact position and orientation of the animal as it moves within its environment. Various methods have been proposed for incorporating both symmetric and asymmetric weights in the continuous attractor, including the introduction of cells that signal rotational velocity to the continuous attractor network (Skaggs et al. 1995; Redish et al. 1996; Samsonovich and McNaughton 1997; Stringer et al. 2002) and imposing the asymmetric weight profile upon the network (Kang 1996; Song and Wang 2005).

An important question is how the network can learn to update the location of the activity packet at the same speed as the animal is moving in its environment during path integration. Even small (but significant) errors in the speed of the packet, compared to the true speed of the animal, could be compounded through time to produce a large discrepancy between the internal representation and the actual location of the animal. In order to achieve successful path integration in a continuous attractor network, there is, thus, a requirement for some biologically plausible mechanism through which the network can self-organize to produce an asymmetry in the synaptic weights that can move the packet of activity in a manner that is calibrated with the speed the animal is moving. We have previously shown how this may be achieved in a biologically plausible manner with Hebbian associative learning, incorporating explicit axonal conduction delays (Walters et al. 2009).

In this article, we demonstrate another way in which this may be achieved, using biologically realistic neuronal time constants to effect natural time delays which are then combined with Hebbian associative learning.

We, thus, propose a model which can learn to update the packet of neural activity at the same speed at which the simulated agent is moving. We address the issue of path integration of head direction, and, therefore, our model is of a generic one-dimensional system. We do, however, note that the general principles of this model could be extended to

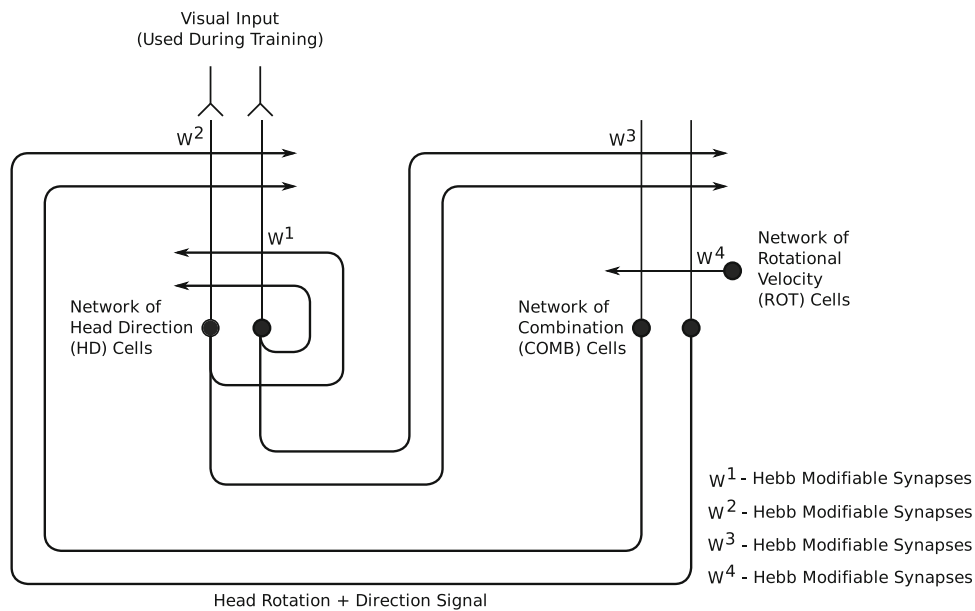


Fig. 1 Network architecture for a two-layer self-organizing neural network model of the head direction system. The model architecture consists of a particular head direction and rotational velocity. In consequence, the combination cells only become active when the agent attains a network of head direction (HD) cells representing the current head direction of the agent; a network of combination (COMB) cells through the Hebb-modifiable  $w_{ij}^2$  synapses. The neuronal time constants introducing effective transmission delays between the head direction and a layer of rotational velocity (ROT) cells that become active when the agent rotates during training, the agent rotates. There are four types of synaptic connectivity in this model, which operate as follows. The  $w_{ij}^1$  synapses are Hebb-modifiable recurrent connections between head direction cells. These connections help to support a stable packet of activity within the continuous attractor network of head direction cells in the absence of visual input. The  $w_{ij}^2$  and  $w_{ij}^3$  synaptic weight profiles, which results in each combination cell learning to stimulate a different postsynaptic head direction cell to the presynaptic head direction cell that has learned to preferentially stimulate it. These asymmetries are important in shifting the packet of combination cells receive inputs from the head direction cells through the Hebb-modifiable  $w_{ij}^3$  synapses, and inputs from the rotational velocity cells through the Hebb-modifiable  $w_{ij}^4$  synapses. These synaptic inputs encourage combination cells to respond, by competitive learning, to

ring rate-based models, as described below. That is, our model does not simulate the individual action potentials emitted by cells. Instead, only the instantaneous average firing rate for each cell is simulated evolving through time. Within the layer of head direction cells, there is a single Gaussian packet of ring activity. The centre of this activity packet represents the current head direction of the simulated agent.

A network of combination cells (with ring rate  $r_i^{COMB}$  for postsynaptic combination cell) receives inputs from both the network of head direction cells and a layer of rotational velocity cells (with separate sub-populations of cells signalling clockwise and counter-clockwise rotation). The combination cells are also simulated using leaky-integrator rate-based models, as described shortly. The combination cells operate as a competitive network and develop their response profiles during training, with individual combination cells learning to represent a combination of a particular head direction and a particular rotational velocity. Such cells have been found in the brain, having both a Gaussian tuning

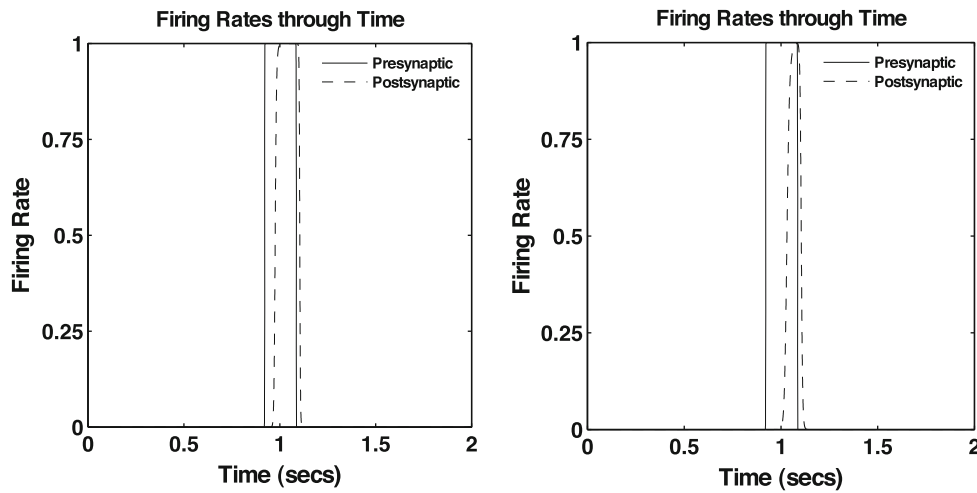


Fig. 2 Firing rates through time of two simulations of a simple two-cell system, with the presynaptic cell ring rate indicated by a solid line and the postsynaptic cell ring rate indicated by a dashed line. Left Simulation in which the time constant of the governing equation for postsynaptic cell activation was set to 50 ms. As can be seen, there is a small delay between the centres of mass of the temporal ring profiles of the presynaptic cell and the postsynaptic cell. Right Simulation in which the time constant of the governing equation for postsynaptic cell activation was set to 100 ms. There is a clear delay between the centres of mass of the temporal ring profiles of the presynaptic cell and the postsynaptic cell. The delay is more pronounced than in the plot, which indicates that a longer time constant will produce a longer delay between the presynaptic and postsynaptic activity profiles

of the presynaptic cell. Although there is a small delay between the centres of mass, the synaptic connection from the presynaptic cell to the postsynaptic cell is still strengthened by the ring rate-based associative Hebbian rule. This learning rule strengthens the connections between the two cells in proportion to the product of their current instantaneous ring rates, and, hence, strengthens the connection during learning because the periods of activity of the two cells still partially overlap through time. This effectively allows the network to learn associations between neural activity in the head direction cell and combination cell networks over specified time intervals  $\Delta t$ , and, thus, the network learns to shift a packet of head direction cell activity at the correct speed.

In order to explain the operation of the model, consider a simple two-cell system. The activation of the postsynaptic cell  $i$  is governed by

$$\tau \frac{dh_i(t)}{dt} = -h_i(t) + w_{ij}(t)r_j(t) \tag{1}$$

where  $\tau$  is the neuronal time constant,  $r_j(t)$  is the ring rate of the presynaptic cell  $j$ , and  $w_{ij}$  is the synaptic weight from the presynaptic cell  $j$  to the postsynaptic cell  $i$ . The ring rate of the postsynaptic cell is given by the sigmoid transfer function

$$r_i(t) = \frac{1}{1 + e^{-2\beta(h_i(t) - \alpha)}} \tag{2}$$

where  $\alpha$  is the sigmoid threshold and  $\beta$  is the slope. Although the presynaptic cell  $j$  and postsynaptic cell  $i$  may be together, a relatively large time constant, say 50–100 ms, will ensure that the centre of mass of the temporal profile

Table 1 Simulation results for the simple two-cell system

Results from two-cell system	
$\tau$ (ms)	$\Delta t$ (ms)
50	36.8
60	43.2
70	49.2
80	54.7
90	59.7
100	64.2

For each of six simulations, we varied the neuronal time constant and measured the effective time delay between the centres of mass of the temporal profile of the presynaptic cell ring and the temporal profile of the postsynaptic cell ring. In relation to the simple model simulated, an increase of 10 ms in the time constant produces an increase of approximately 5–6 ms in the time delay between the centres of mass of the presynaptic and postsynaptic cell temporal ring profiles

of the postsynaptic cell activity is delayed by a small time interval  $\Delta t$  from the centre of mass of the temporal profile of the presynaptic cell activity. A larger neuronal time constant  $\tau$  will lead to a longer effective delay  $\Delta t$ . This is shown in Fig. 2 and Table 1.

During learning, the synaptic weight  $w_{ij}$  from presynaptic cell  $j$  to postsynaptic cell  $i$  is strengthened according to the Hebbian associative learning rule

$$\frac{dw_{ij}(t)}{dt} = kr_i(t)r_j(t) \tag{3}$$

where  $k$  is the learning rate,  $r_j$  is the ring rate of the presynaptic cell, and  $r_i$  is the ring rate of the postsynaptic cell. This

learning rule depends upon the instantaneous firing rates of the presynaptic and postsynaptic cells, and does not depend upon the precise timing of the action potentials emitted by these cells (which are not explicitly simulated in this model).

Now let us reconsider the full model, shown in Fig. 1, that is simulated in this paper. In the simulations presented below we implemented relatively large neuronal time constants  $\tau^{COMB} = 100$ – $150$  ms for the combination cells, and a relatively small time constant  $\tau^{HD} = 1$  ms for the head direction cells. This meant that the main effective delay in neurotransmission was in the head direction cell to combine the presynaptic cell with a slightly delayed temporal activity profile in the postsynaptic cell. In particular, the input is available to guide the firing of the head direction centre of mass of the temporal activity profile of the postsynaptic cell is always delayed  $\Delta t$  from the centre of mass of their preferred head direction. At any moment in time the temporal activity profile of the presynaptic cell. This will individual combination cells will respond to an earlier pattern true both during and after learning. The consequence of this is that the presynaptic cell learns to drive activity in the postsynaptic cell with the same effective time delay that was present during learning. Moreover, a longer postsynaptic time constant ensures that the presynaptic cell learns to stimulate the postsynaptic cell a greater time interval  $\Delta t$  after the presynaptic cell firing. It is this delay between presynaptic and postsynaptic cell firing, which allows the correct time intervals between cell activities to be learned and replayed by cells in the model. This is essential for the model to be able to replay the temporal sequence of cell activity at the speed that was experienced during learning.

In order to further illustrate how the neuronal time constant leads to effective signal delays, we simulated a two-cell system according to Eqs 1 and 2 with a non-modifiable synaptic weight  $w_{ij} = 1$  between the presynaptic and postsynaptic cells. Figure 2 displays the presynaptic and postsynaptic cell firing rates through time for two simulations of the two-cell system. In the left plot, the neuronal time constant  $\tau$  for the postsynaptic cell was set to 50 ms. It is evident that there is a delay between the temporal profiles of the presynaptic cell and the postsynaptic cell. In the right plot, the neuronal time constant was set to 100 ms. The delay between the presynaptic and postsynaptic cell firing is more pronounced, which illustrates that a longer time constant will produce a longer delay  $\Delta t$  between the presynaptic and postsynaptic temporal activity profiles. In order to further quantify this mechanism, we conducted six simulations of the two-cell system, each with different values for the time constant. For each simulation, we calculated the time delays  $\Delta t$  between the centres of mass of the presynaptic cell temporal firing profile and the postsynaptic cell temporal firing profile. Table 1 shows the calculated delays for the six simulations conducted with different values of the postsynaptic neuronal time constant. Each increase of 10 ms in the time constant leads to an approximate increase of 5–6 ms in the effective delay  $\Delta t$ . These results show that the time delay is approximately proportional to the neuronal time constant  $\tau$ . The time constant can, thus, serve as a reliable timing

mechanism over which associations can be made between presynaptic and postsynaptic cell activities. Now let us reconsider the full model, shown in Fig. 1, that is simulated in this paper. In the simulations presented below we implemented relatively large neuronal time constants  $\tau^{COMB} = 100$ – $150$  ms for the combination cells, and a relatively small time constant  $\tau^{HD} = 1$  ms for the head direction cells. This meant that the main effective delay in neurotransmission was in the head direction cell to combine the presynaptic cell with a slightly delayed temporal activity profile in the postsynaptic cell. In particular, the input is available to guide the firing of the head direction centre of mass of the temporal activity profile of the postsynaptic cell is always delayed  $\Delta t$  from the centre of mass of their preferred head direction. At any moment in time the temporal activity profile of the presynaptic cell. This will individual combination cells will respond to an earlier pattern true both during and after learning. The consequence of this is that the presynaptic cell learns to drive activity in the postsynaptic cell with the same effective time delay that was present during learning. Moreover, a longer postsynaptic time constant ensures that the presynaptic cell learns to stimulate the postsynaptic cell a greater time interval  $\Delta t$  after the presynaptic cell firing. It is this delay between presynaptic and postsynaptic cell firing, which allows the correct time intervals between cell activities to be learned and replayed by cells in the model. This is essential for the model to be able to replay the temporal sequence of cell activity at the speed that was experienced during learning.

work at time  $t_1$  representing a particular head direction  $\theta_1$  should stimulate (via the network of combination cells) a new pattern of activity in the head direction cell network at time  $t_2 = t_1 + \Delta t$ , representing a later head direction  $\theta_2 = \theta_1 + \Delta t \frac{d\theta}{dt}$ . This kind of associative learning over extended time intervals enables the model to learn the correct velocity for updating the packet of neural activity in the head direction cell network, and thus allows path integration to occur at the correct speed.

## 2.2 Model equations and implementation

The two-layer model architecture is shown in Fig. 1. During training, each head direction cell receives an external visual input  $e_i$ , which carries information about the head direction of the agent. When visual cues are available, these external inputs dominate other excitatory inputs to the head direction cells, and force each head direction cell to respond best to a particular head direction of the agent. The Gaussian tuning of the head direction cell response profile leads, for any given head direction cell, to a decrease in cell firing as the head direction of the agent moves away from the preferred head direction of that cell.

The activation  $h_i^{HD}$  of head direction  $i$  in the model is governed by

$$\tau^{HD} \frac{dh_i^{HD}(t)}{dt} = -h_i^{HD}(t) + e_i(t) - \frac{1}{N^{HD}} \sum_j \tilde{w}_{ij}^{HD} r_j^{HD}(t)$$

$$\begin{aligned}
 & + \frac{\phi_1}{C^{\text{HD} \rightarrow \text{HD}}} \sum_j w_{ij}^1(t) r_j^{\text{HD}}(t) \\
 & + \frac{\phi_2}{C^{\text{COMB} \rightarrow \text{HD}}} \sum_j w_{ij}^2(t) r_j^{\text{COMB}}(t) \\
 & - I^{\text{EXTERN}}
 \end{aligned} \tag{4}$$

$$r_i^{\text{HD}}(t) = \frac{1}{1 + e^{-2\beta(h_i^{\text{HD}}(t) - \alpha)}} \tag{5}$$

where  $\alpha$  and  $\beta$  are the sigmoid threshold and slope respectively.

The recurrent synapses  $w_{ij}^1(t)$  in the head direction cell network are trained by a local associative Hebb rule

where the activation  $r_i^{\text{HD}}(t)$  is driven by the following terms:

$$\frac{dw_{ij}^1(t)}{dt} = k^1 r_i^{\text{HD}}(t) r_j^{\text{HD}}(t) \tag{6}$$

$\sum_j \bar{w}_{ij}^{\text{HD}} r_j^{\text{HD}}(t)$  represents inhibitory feedback within the head direction cell network, where the summation is performed over all the presynaptic head direction cells.  $\bar{w}^{\text{HD}}$  is a global constant describing the effect of inhibitory interneurons within the network of head direction cells, and  $N^{\text{HD}} = 500$  is the total number of head direction cells in the model. The term  $\sum_j w_{ij}^1(t) r_j^{\text{HD}}(t)$  represents excitatory feedback within the layer of head direction cells. The term  $r_j^{\text{HD}}(t)$  is the presynaptic firing rate of head direction cell  $j$  and  $w_{ij}^1$  is the excitatory (positive) synaptic weight from presynaptic head direction cell  $j$  to postsynaptic head direction cell  $i$ . Further terms in Eq. 4 are as follows. The term  $h_i^{\text{HD}}(t)$  is a decay term such that, in the absence of further presynaptic input, the activation level of the postsynaptic head direction cell will decay to zero according to the time constant  $\tau^{\text{HD}}$ .

The term  $e_i(t)$  represents an external visual input to postsynaptic head direction cell  $i$ . When there is no visual input, the term  $e_i$  is set to zero. Thus, in the absence of visual input, the key term driving the head direction cell activations in Eq. 4 is a sum of inputs from the presynaptic combination cells  $\sum_j w_{ij}^2(t) r_j^{\text{COMB}}(t)$ . The term  $r_j^{\text{COMB}}(t)$  is the firing rate of the presynaptic combination cell  $j$  and  $w_{ij}^2$  is the strength of the corresponding synapse between that presynaptic combination cell and the postsynaptic head direction cell  $i$ . The term  $I^{\text{EXTERN}}$  represents external feedforward inhibition to the head direction cell network: this is necessary during the learning phase to ensure that, in the presence of visual input, only a small subset of head direction cells (those representing head directions nearby in the head-direction space) are active at any one point in time, i.e. the standard deviation of the head direction cell activity packet remains small. In the absence of external visual input (during the testing phase) the term  $I^{\text{EXTERN}}$  is set to zero.

The firing rate  $r_i^{\text{HD}}(t)$  of postsynaptic head direction cell  $i$  is determined from the activation  $h_i^{\text{HD}}(t)$  of that cell and the sigmoid activation function

$$\sqrt{\sum_j (w_{ij}^1(t))^2} = 1 \tag{7}$$

where the sum is over all the presynaptic head direction cells  $j$ . Such a renormalization process may be achieved in biological systems through synaptic weight decay (Aja 1982; Rolls and Treves 1998). The renormalization helps in ensuring that the learning rules are convergent in the sense that the recurrent synaptic weights within the continuous attractor network settle down over time to steady values, i.e. the weights do not grow unbounded.

During learning, associative synaptic modification in the recurrent synapses  $w_{ij}^1$ , in conjunction with the continuity of the head-direction space, allows the strength of the synapses between any two head direction cells to reflect the distance between the head directions represented by those two cells. The recurrent connectivity implemented by the synapses allows the network of head direction cells to operate as a continuous attractor network and support stable packets of neural activity in the absence of external visual input; thus, the agent can operate in the dark.

The learning rule to update the  $w_{ij}^2(t)$  synapses from presynaptic combination cell  $j$  to postsynaptic head direction cell  $i$  is expressed by

$$\frac{dw_{ij}^2(t)}{dt} = k^2 r_i^{\text{HD}}(t) r_j^{\text{COMB}}(t) \tag{8}$$

which increases the strength of the synapses between co-active postsynaptic head direction cells and presynaptic combination cells. In order to bound the  $w_{ij}^2(t)$  synaptic weights, rescaling occurred after each timestep of the learning phase, as in Eq. 7, to ensure that for each postsynaptic head direction cell  $i$ , we have

<sup>1</sup> The scaling factor  $\frac{\phi_1}{C^{\text{HD} \rightarrow \text{HD}}}$  controls the overall strength of the recurrent inputs to the network of head direction cells, where  $\phi_1$  is a constant, and  $C^{\text{HD} \rightarrow \text{HD}}$  is the number of synapses onto each postsynaptic head direction cell from the presynaptic head direction cells.

<sup>2</sup> The scaling factor  $\frac{\phi_2}{C^{\text{COMB} \rightarrow \text{HD}}}$  controls the overall strength of the combination cell inputs, where  $\phi_2$  is a constant, and  $C^{\text{COMB} \rightarrow \text{HD}}$  is the number of synapses onto each postsynaptic head direction cell from the presynaptic combination cells.

$$\sqrt{\sum_j (w_{ij}^2(t))^2} = 1 \tag{9}$$

where the sum is over all the presynaptic combination cells  $j$ .

After learning has occurred, and during testing in the absence of visual input, the  $w_{ij}^2$  synapses are responsible for stimulating new head direction cells in the direction the agent is rotating, so as to shift the location of the head direction cell activity packet and, thus, perform path integration.

The combination cells are driven by synaptic inputs from the head direction cell network, and synaptic inputs  $w_{ij}^4(t)$  from the layer of rotational velocity cells (which are external inputs to the network that are only active when the agent is rotating). During the training phase,  $w_{ij}^3$  and  $w_{ij}^4$  synapses onto the combination cells self-organize using Hebbian competitive learning rules, which enable the combination cell network to operate as a competitive network that learns to represent different combinations of a particular head direction and rotational velocity. The activation of the postsynaptic combination cells is governed by

$$\begin{aligned} \tau_{\text{COMB}} \frac{dh_i^{\text{COMB}}(t)}{dt} = & -h_i^{\text{COMB}}(t) \\ & - \frac{1}{N_{\text{COMB}}} \sum_j \tilde{w}^{\text{COMB}} r_j^{\text{COMB}}(t) \\ & + \frac{\phi_3}{C_{\text{HD} \rightarrow \text{COMB}}} \sum_j w_{ij}^3(t) r_j^{\text{HD}}(t) \\ & + \frac{\phi_4}{C_{\text{ROT} \rightarrow \text{COMB}}} \sum_j w_{ij}^4(t) r_j^{\text{ROT}}(t) \end{aligned} \tag{10}$$

with the terms defined as follows. The term  $\sum_j \tilde{w}^{\text{COMB}} r_j^{\text{COMB}}(t)$  represents inhibitory feedback within the combination cell network, where the summation is performed over all postsynaptic combination cells  $j$ .  $\tilde{w}^{\text{COMB}}$  is the global lateral inhibition constant describing the effect of inhibitory interneurons within the combination cell network, and  $N_{\text{COMB}} = 1000$  is the total number of combination cells in the model. The term  $\sum_j w_{ij}^3(t) r_j^{\text{HD}}(t)$  is the input from the head direction cells, where  $r_j^{\text{HD}}(t)$  is the firing rate of presynaptic head direction cell  $j$ , and  $w_{ij}^3(t)$  is the corresponding strength of the synapse from this cell. The term  $\sum_j w_{ij}^4(t) r_j^{\text{ROT}}(t)$  is the input from the rotational velocity cells, where the firing rate of presynaptic rotational velocity cell  $j$  is given by  $r_j^{\text{ROT}}(t)$ , and  $w_{ij}^4(t)$  is the strength of the corresponding syn-

apse from this cell. Activity within the combination cell network is driven by the head direction cell network if, and only if, the rotational velocity cells are also active. If the rotational velocity cells cease firing, i.e. the agent is stationary, then the activity in the combination cell network decays to zero according to the term  $h_i^{\text{COMB}}(t)$  and the time constant  $\tau_{\text{COMB}}$ .

The firing rate  $r_i^{\text{COMB}}(t)$  of postsynaptic combination cell is determined from the activation  $h_i^{\text{COMB}}(t)$  and the sigmoid activation function

$$r_i^{\text{COMB}}(t) = \frac{1}{1 + e^{-2\beta(h_i^{\text{COMB}}(t) - \alpha)}} \tag{11}$$

where  $\alpha$  and  $\beta$  are the sigmoid threshold and slope, respectively. The threshold  $\alpha$  is set to a high value to ensure that each individual postsynaptic combination cell will function similar to a logical AND gate. That is to say that temporally conjunctive inputs from the presynaptic head direction cells and presynaptic rotational velocity cells are required in order for the postsynaptic combination cells to fire. In this manner, individual combination cells become selective to combinations of a particular head direction occurring a small time interval  $\Delta t$  in the past and a rotational velocity, and, thus, a competitive network emerges.

The synaptic weights  $w_{ij}^3(t)$  from the head direction cells to the combination cells are updated during learning according to

$$\frac{dw_{ij}^3(t)}{dt} = k^3 r_i^{\text{COMB}}(t) r_j^{\text{HD}}(t) \tag{12}$$

which increases the strength of the synapses between co-active presynaptic head direction cells and postsynaptic combination cells. In order to bound the synaptic weights, rescaling was employed after each timestep of the learning phase to ensure that for each postsynaptic combination cell  $i$ , we have

$$\sqrt{\sum_j (w_{ij}^3(t))^2} = 1 \tag{13}$$

where the sum is over all presynaptic head direction cells  $j$ .

The synaptic weights  $w_{ij}^4(t)$  from the rotational velocity cells to the combination cells are updated during learning according to

$$\frac{dw_{ij}^4(t)}{dt} = k^4 r_i^{\text{COMB}}(t) r_j^{\text{ROT}}(t) \tag{14}$$

and the weights are bound by rescaling after each timestep of learning to ensure that for each postsynaptic combination

<sup>3</sup> The scaling factor  $\frac{\phi_3}{C_{\text{HD} \rightarrow \text{COMB}}}$  controls the overall strength of the inputs from the head direction cells, where  $\phi_3$  is a constant, and  $C_{\text{HD} \rightarrow \text{COMB}}$  is the number of synapses onto each postsynaptic combination cell from the presynaptic head direction cells.

<sup>4</sup> The scaling factor  $\frac{\phi_4}{C_{\text{ROT} \rightarrow \text{COMB}}}$  controls the overall strength of the inputs from the rotational velocity cells, where  $\phi_4$  is a constant, and  $C_{\text{ROT} \rightarrow \text{COMB}}$  is the number of synapses onto each postsynaptic combination cell from the presynaptic rotational velocity cells.

Table 2 Simulation parameter values (values are constant across all experiments except where specified)

Network parameters	
No. HD cells	500
No. COMB cells	1000
No. ROT cells	500
No. $w^1$ synapses onto each HD cell	500
No. $w^2$ synapses onto each HD cell	1000
No. $w^3$ synapses onto each COMB cell	25
No. $w^4$ synapses onto each COMB cell	500
$\bar{w}^{HD}$	375
$\bar{w}^{COMB}$	50
$J^{EXTERN}$	150
$\sigma^{HD}$	20°
Learning rates $k^1, k^2, k^3, k^4$	0.1
$\lambda$	200.0
$\tau^{HD}$	1.0 ms
$\tau^{COMB}$ (Experiments 1 and 2)	150.0 ms
$\tau^{COMB}$ (Experiments 3 and 4)	100.0 ms
$\phi_1$	$3.75 \times 10^3$
$\phi_2$	$2.5 \times 10^3$
$\phi_3$	$5 \times 10^3$
$\phi_4$	$4 \times 10^2$
HD sigmoid transfer function parameters	
$\alpha$	0.0
$\beta$	1.5
COMB sigmoid transfer function parameters	
$\alpha$	10.0
$\beta$	1.5
Training parameters	
No. Training epochs	50
Speed of rotation (Experiments 1 and 3)	360
Speed of rotation (Experiments 2 and 4)	180

HD Head direction, COMB Combination, ROT Rotational velocity

cell  $i$  we have

$$\sqrt{\sum_j (w_{ij}^4(t))^2} = 1 \tag{15}$$

where the sum is over all presynaptic rotational velocity cells  $j$ .

During training, the  $w_{ij}^3$  and  $w_{ij}^4$  synapses onto the postsynaptic combination cells self-organize using competitive learning to enable the combination cells to learn to represent combinations of particular head directions and rotational velocities.

In the models simulated, we set the neuronal time constant  $\tau^{COMB}$  for the combination cells to a large value as given in Table 2. This was due to the results from some preliminary

simulations, which indicated that having a relatively large time constant  $\tau^{COMB}$  compared to the neuronal time constant  $\tau^{HD}$  for the head direction cells would produce the best operation of the model. The large value of the time constant  $\tau^{COMB}$  means that, through learning, the current activity in the combination cell network will be associated with activity that occurred  $\Delta t$  in the past in the head direction cell network due to the effective time delay  $\Delta t$  between the activity packet in the head direction cell network and the activity in the combination cell network. Thus, after unsupervised learning, different cells in the combination cell network will respond to different combinations of a particular head direction that occurred  $\Delta t$  in the past and a rotational velocity (i.e. direction of movement through the head-direction space).

### 2.3 Training and testing

In order to keep the simulation run-time reasonable, the models were simulated with a relatively small architecture containing 500 head direction cells and 1000 combination cells. There were also 500 rotational velocity cells—with 250 of the cells (1–250) responding to clockwise rotation of the agent, and the remaining 250 cells (251–500) responding to counter-clockwise rotation. The head direction cells were mapped onto a regular grid of different head directions, such that each postsynaptic head direction cell had a preferred head direction  $x_i$  of the agent at which the cell would be maximally stimulated by the visual input.

Throughout the training phase, the agent moved round a 1D circular space. A full clockwise rotation of the agent through consecutive positions 0–360 followed by a full counter-clockwise rotation of the agent through consecutive positions 360–0 constituted 1 epoch of training. The training phase was complete after 50 epochs had been performed. As the agent rotated during training, the activations and firing rates of the head direction cells were simulated according to the dynamical Eqs 4 and 5.

During training in the light, the external visual inputs included in Eq 4, were the dominant influence upon the firing of the head direction cells. Since each head direction cell is tuned to respond maximally to visual input from a particular head direction, for each postsynaptic cell the visual input  $e_i$  was set to the following Gaussian response profile

$$e_i^{HD} = \lambda e^{-(s_i^{HD})^2 / 2(\sigma^{HD})^2} \tag{16}$$

where  $s_i^{HD}$  is the difference between the actual head direction  $x$  of the agent and the preferred head direction  $x_i$  of the postsynaptic head direction cell  $\lambda$  is a scaling factor that

expresses the strength of the non-modifiable visual input synapses onto the postsynaptic head direction cells, and  $\sigma^{HD}$  is the standard deviation. For each postsynaptic head direction



cell  $i$ , the difference  $\alpha_i^{HD}$  is given by

$$s_i^{HD} = \text{MIN}(|x_i - x|, 360 - |x_i - x|). \tag{17}$$

In the training phase of the simulations, the activity of the combination cells is driven by the  $w_{ij}^3$  synaptic inputs from the presynaptic head direction cells, and the  $w_{ij}^4$  synaptic inputs from the rotational velocity cells. One of the purposes of the training phase was to determine that the model can self-organize, through competitive learning, to correctly set up the combination cells to respond to combinations of a particular head direction occurring in the past and clockwise or counter-clockwise rotation. Throughout the training, the activations and the ring rates of the combination cells were simulated according to the dynamical Eqs. 9 and 11.

At the beginning of the training phase, the synaptic weights  $w_{ij}^1$ ,  $w_{ij}^2$ ,  $w_{ij}^3$  and  $w_{ij}^4$  were all initialized to random positive values. These weights were updated at every timestep of the training phase according to Eqs. 8, 12, and 14, respectively, and thus allowed to self-organize.

After the training phase was over, the simulations continued with the testing phase, during which the packet of head direction cell activity was required to update on the basis of idiothetic signals alone (the visual inputs were set to zero). During the testing phase, the dynamical Eqs. 10 and 11 were simulated, but without any learning in any of the synapses i.e. Eqs. 8, 12 and 14 were not simulated.

At the start of the testing phase, all of the ring rates  $r_i^{HD}$ ,  $r_i^{COMB}$  and  $r_i^{ROT}$  were set to zero. The agent was oriented to an initial head direction and simulated with visual input available, but with no rotational velocity cells being active, for a period of 1 s. For the period that the agent maintained this head direction, the visual input term for each postsynaptic head direction cell was set to a Gaussian response of visual input. The model parameters used for this experiment are identical to that used by the head direction cell during the training phase as given by Eq. 6. The visual input was then removed by setting all the terms to zero, and the agent was allowed to rest in the same initial head direction for a further 1 s. The purpose of this initial part of the testing was to allow the development within the head direction cell network of a stable packet of activity (representing the initial head direction).

The agent was allowed to remain stationary for a further 1 s, then the ring rates  $r_i^{ROT}$  of the 250 clockwise rotational velocity cells were set to 1 (fully active) for 1 s. The combination cell network. The ring of these combination cells then stimulated cells in the head direction cell network representing ing head directions in the clockwise direction of rotation, and the packet of head direction cell activity moved through the continuous attractor. This part of the testing phase was

to ascertain that the representation of current head direction can be updated on the basis of idiothetic signals alone.

The ring rates  $r_i^{ROT}$  of all the rotational velocity cells were then set to 0 for 1 s. As the 250 clockwise rotational velocity cells ceased ring, the driving input to the combination cells disappeared, and the combination cells also ceased ring. In consequence, the combination cell network no longer provided a driving input to the head direction cell network, and the packet of head direction cell activity remained stationary at the last-visited head direction. This was to demonstrate that the head direction cell network could maintain a stable packet of activity representing any given head direction.

The ring rates  $r_i^{ROT}$  of the 250 counter-clockwise rotational velocity cells were then set to 1 for 1 s. In an identical manner to the period of clockwise rotation, the head direction cell activity packet then updated in a counter-clockwise direction, to demonstrate that counter-clockwise rotation could also be achieved on the basis of idiothetic signals alone.

The ring rates  $r_i^{ROT}$  of all the rotational velocity cells were then set to 0 for a final 1 s. Again, this was to demonstrate that the head direction cell network could maintain a stable packet of activity at the last-visited head direction.

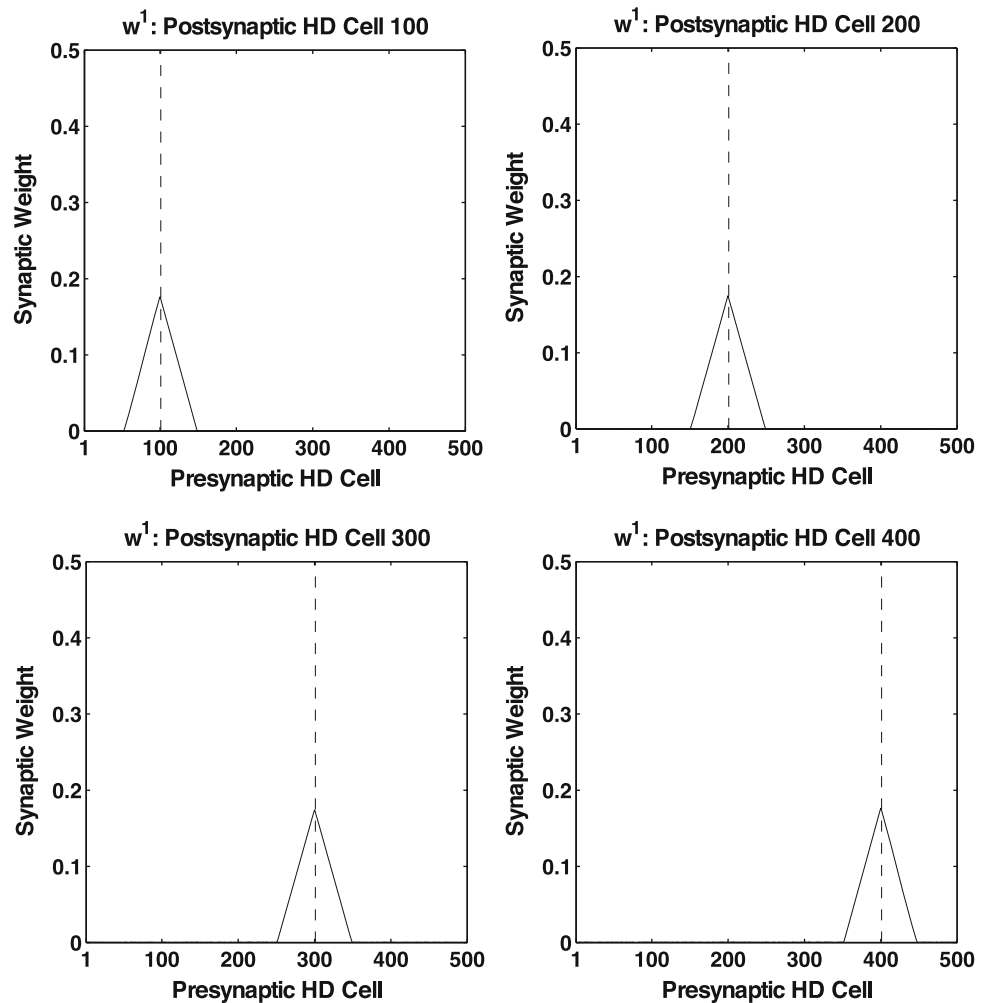
In the simulations, all the differential Eqs. 6, 8, 10, 12, 14 were approximated by Forward Euler finite difference schemes with a timestep of 0.0001 s.

### 3 Simulations

**3.1 Experiment 1**  $\tau^{COMB}$  150 ms; 360°/s rotational velocity  
 In this experiment, the model was simulated with the agent rotating at a velocity of 360°/s during training in the presence of visual input. The model parameters used for this experiment are given in Table 2. Testing in the absence of visual input was then carried out to determine whether the model had learned to update a packet of head direction cell activity at the same speed as the rotational velocity imposed during training. The results from the testing phase are shown in Figs. 3 to 7, and also in Table 3.

Figure 3 displays the recurrent synaptic weights within the head direction cell network after training with the corresponding Hebbian associative learning rule (Eq. 6) and weight normalization (7). Each of the four plots shows the learned synaptic weights to a different postsynaptic head direction within each plot, the presynaptic head direction cells are arranged according to where they are maximally in the head-direction space of the agent when visual input is available. In each plot, a dashed vertical line indicates the presynaptic head direction cell with which the postsynaptic head direction cell has a maximal  $w^1$  synaptic weight. For all the plots, the syn-

Fig. 3 The recurrent synaptic weights  $w^1$  within the network of head direction (HD) cells after training with the Hebbian associative learning rule (6) and weight normalization (7). These results are from a simulation with a time constant  $\tau^{COMB}$  of 150 ms, and a rotational velocity during training of 360/s (all other parameters are as given in Table 2). Each of the four plots shows the learned synaptic weights to a different postsynaptic HD cell from the other 500 presynaptic HD cells in the network. In the plots, the 500 presynaptic HD cells are arranged according to where they are maximally in the head-direction space of the agent when visual input is available. For each plot, a dashed vertical line indicates the presynaptic HD cell with which the postsynaptic HD cell has maximal  $w^1$  synaptic weight. In all the plots, the synaptic weight profile is symmetric about the presynaptic HD cell with maximal synaptic strength, and this symmetry helps in supporting a stable packet of HD cell activity during testing in the absence of visual input



aptic weight profile across the presynaptic head direction combination of a particular head direction occurring in cells is clearly symmetric about the individual presynaptic the past and a rotational velocity, rather than all possible head direction cell with maximal  $w^1$  synaptic strength. This head directions due to the continuity of the head-direction symmetry ensures that the head direction cell network can space and the overlapping receptive fields of the head direction maintain a stable packet of head direction cell activity when cells (Stringer and Rolls 2006) With the exception of the agent is stationary in the absence of visual input. this diluted connectivity, each of the synaptic weight profiles is centred on a region of similarly tuned head direction

In Fig. 4, the plots display the  $w^3$  synaptic weights from the head direction cell network to the combination cells and is approximately symmetric about the presynaptic network after competitive learning with the corresponding head direction cell with maximal  $w^3$  synaptic weight. The associative Hebbian learning rule (12) and weight normalization (13). Each individual plot shows the learned synaptic weights to a different postsynaptic combination cell from by a subset of presynaptic head direction cells representing the 500 presynaptic head direction cells, with the presynaptic preferred head direction  $\theta$  in the past. Since the model head direction cells arranged in the plots according to where parameters  $\phi_3$ ,  $\phi_4$  and the threshold  $\theta$  of the combination they are maximally in the head-direction space of the agent in cell sigmoid transfer function  $f(\theta)$  are tuned to ensure that a the presence of visual input. For each plot, a dashed vertical line indicates the presynaptic head direction cell with which the postsynaptic combination cell has maximal synaptic strength. Diluted synaptic connectivity was implemented combinations of a particular head direction  $\theta$  in the past and for the  $w^3$  synapses to ensure that competitive learning was clockwise or counter-clockwise rotational velocity. preserved in the combination cell network. Thus, individual The plots in Fig 5 display the synaptic weights  $w^2$  from ual postsynaptic combination cells learned to respond to the combination cell network to the head direction cell net-

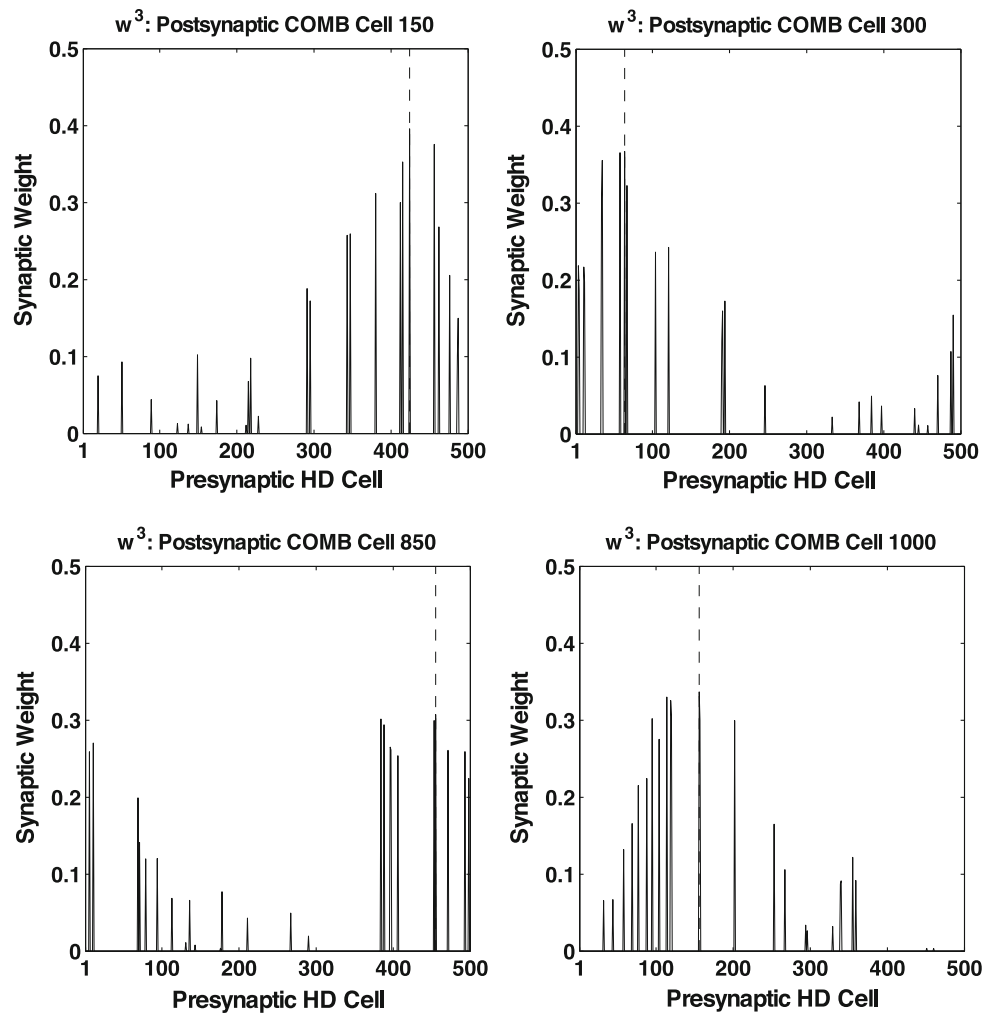


Fig. 4 The synaptic weights  $w^3$  from the head direction (HD) cell network to the combination (COMB) cell network after competitive learning with the Hebbian associative learning rule (8) and weight normalization (13). These results are from a simulation with a time constant  $\tau^{COMB}$  of 150 ms, and a rotational velocity of 360°/s (all other parameters are as given in Table 1). Each of the four plots shows the learned synaptic weights to a different postsynaptic COMB cell from the 500 presynaptic HD cells. The presynaptic HD cells are arranged in the plots according to where they are maximally in the head-direction space of the agent when visual input is available. For each plot, a dashed vertical line indicates the presynaptic HD cell with which the postsynaptic COMB cell has maximal weight. Except for the effects of diluted synaptic connectivity, each of the weight profiles is centred on a region of similarly tuned HD cells, with a profile that is approximately symmetric about the presynaptic HD cell with maximal synaptic strength. Thus, the learned synaptic weights show that individual COMB cells learn to receive maximal stimulation from particular HD cells. Given that the model parameters  $\phi_4$ , and the threshold  $\alpha$  of the COMB cell sigmoid transfer function (1) are tuned to ensure that strong rotational velocity cell input through the synapses is also needed to fire the COMB cells, these cells in fact learn to respond to combinations of a particular head direction and clockwise or counter-clockwise rotational velocity

work after learning with the corresponding Hebbian association combination cell has maximal  $w^3$  weight as per Fig. 4. For all competitive learning rule (8) and weight normalization (9). In all four plots, the  $w^2$  synaptic weight profile is asymmetric about each plot, the learned synaptic weights are shown from a different postsynaptic head direction cell with maximal weight. This asymmetry shows that the presynaptic combination cell has learned to preferentially stimulate a postsynaptic head direction cell that represents a different head direction to the head-direction space of the agent when visual input is available. The dashed vertical lines indicate, for each plot, the presynaptic head direction cell from which the combination cell receives maximal  $w^3$  stimulation. Thus, the asymmetry reflects the fact that, during training in the presence of visual input, the

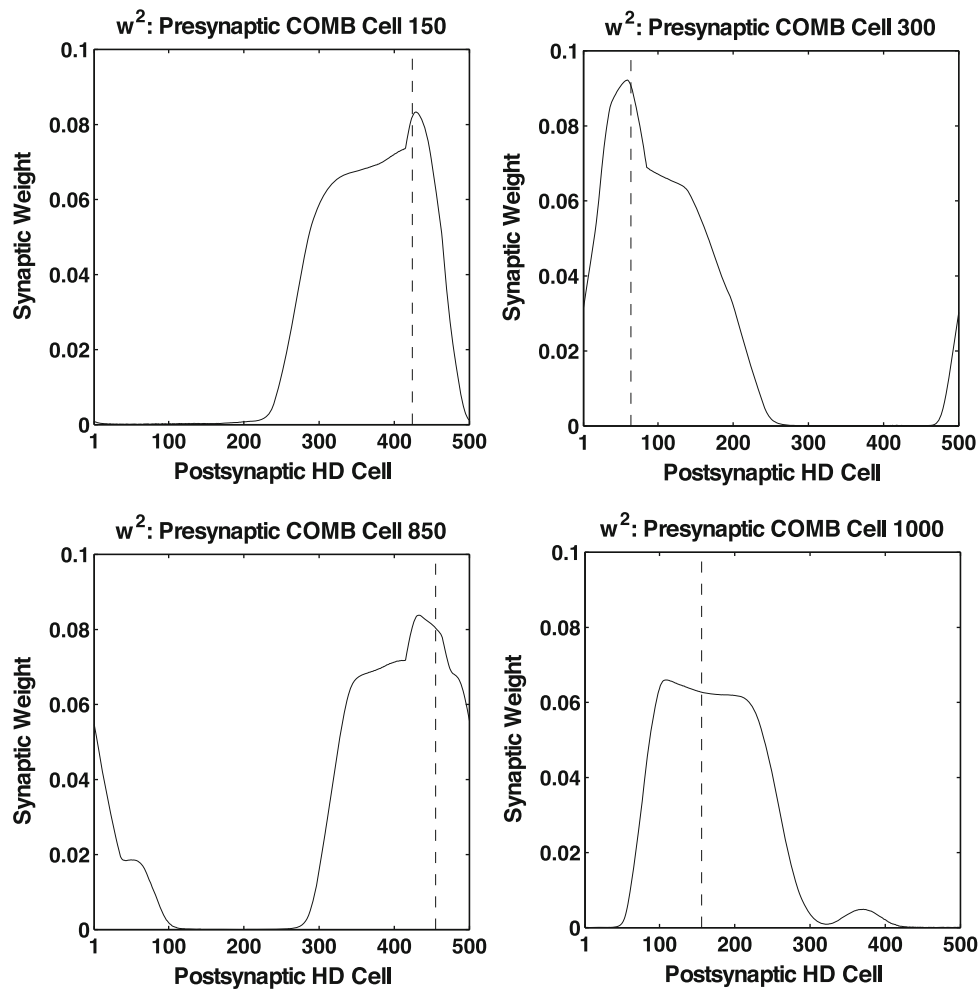
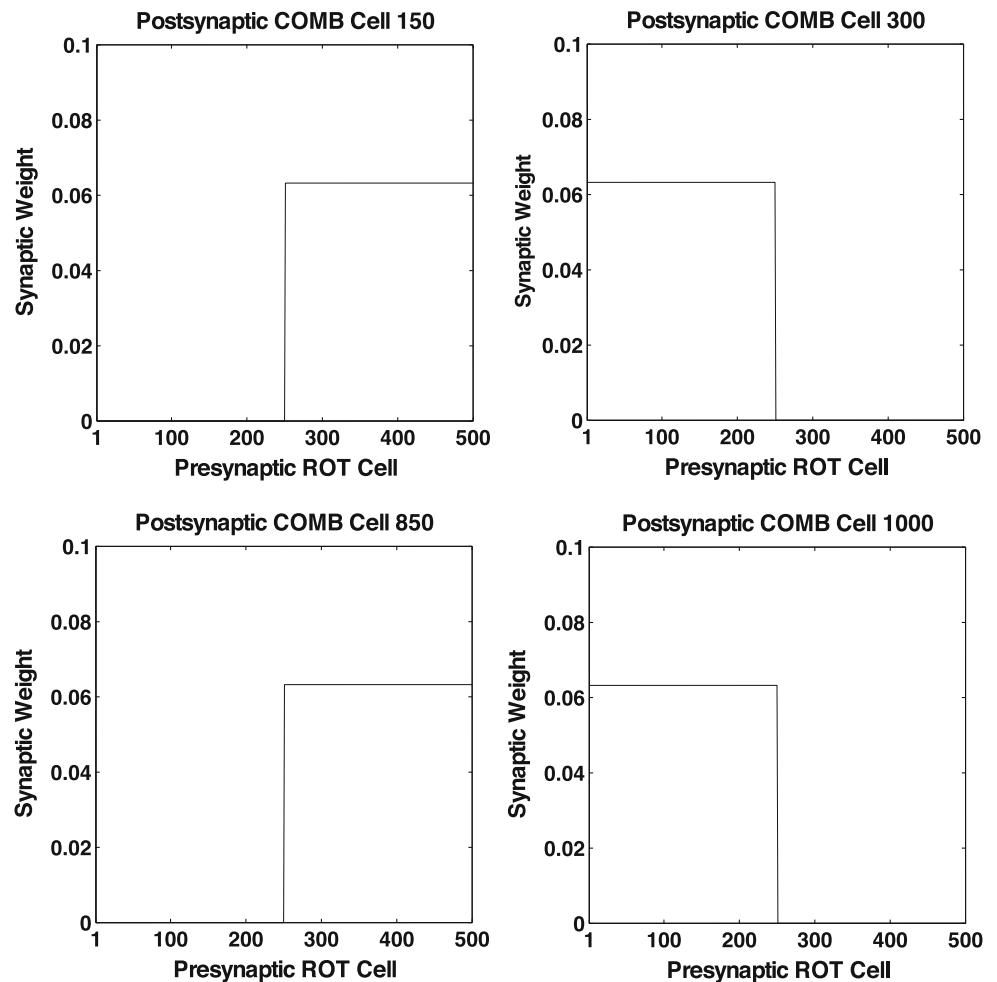


Fig. 5 The synaptic weights  $w^2$  from the combination (COMB) cell network to the head direction (HD) cell network after learning with the Hebbian associative learning rule (4) and weight normalization (5). These results are from a simulation with a time constant  $\tau^{COMB}$  of 150 ms, and a rotational velocity of 360° (all other parameters are as given in Table 6). Each of the four plots shows the learned synaptic weights from a different presynaptic COMB cell to the 500 postsynaptic HD cells. The postsynaptic HD cells are arranged in the plots according to where they are maximally in the head-direction space of the agent when visual input is available. For each plot, a dashed vertical line indicates the postsynaptic HD cell with which the presynaptic COMB cell has maximal  $w^3$  weight as shown in Fig. 4. In each plot, the  $w^2$  synaptic weight profile is asymmetric about the postsynaptic HD cell with maximal  $w^3$  synaptic weight, indicating that the presynaptic COMB cell preferentially stimulates an HD cell representing a different head direction to the HD cell from which the COMB cell receives maximal  $w^3$  synaptic weight. This reflects the fact that the packet of weights from a different presynaptic COMB cell to the 500 postsynaptic HD cells and the resulting ring of the postsynaptic combination cells. Thus, the effective natural time delays produced by the neuronal time constants  $\tau^{COMB}$  and  $\tau^{HD}$  act, through learning, as a timing mechanism that enables the update of the packet of HD cell activity at the same speed as the agent is rotating

packet of head direction cell activity (representing current head direction) will have moved through the head-direction space of the agent in the natural time delay between the activity profile in the head direction cell network and the activity profile in the combination cell network. This results, at any given moment in time, in the most active combination cell learning to stimulate a different postsynaptic head direction cell to the presynaptic head direction cell it has learned to be stimulated by, reflecting the changing head directions of the agent. Therefore, the neuronal time constants  $\tau^{COMB}$  and  $\tau^{HD}$  act, through learning, as a timing mechanism that is sufficient for the purpose of enabling the update of the packet of head direction cell activity at the same speed as the agent is rotating. Figure 6 displays the  $w^4$  synaptic weights from the layer of rotational velocity cells to the combination cell network after learning with the corresponding Hebbian associative learning rule (14) and weight normalization (5). Each of the plots shows the learned synaptic weights to a different postsynaptic combination cell from the 500 presynaptic rotational veloc-

Fig. 6 The synaptic weights  $w^4$  from the layer of rotational velocity (ROT) cells to the combination (COMB) cell network after learning with the Hebbian associative learning rule (14) and weight normalization (15). These results are taken from a simulation with a time constant  $\tau^{\text{COMB}}$  of 150 ms, and a rotational velocity of 360°/s (all other parameters are as given in Table 2). Each of the four plots shows the learned synaptic weights to a different postsynaptic COMB cell from the 500 presynaptic ROT cells. As the ring profile of the presynaptic ROT cells is binary, the  $w^4$  synaptic weight profiles in the plots above can be described as a step function of the presynaptic ROT cell ring rate  $r_j^{\text{ROT}}(t)$ . Combination cells 300 and 1000 have learned to respond to the clockwise direction of rotation. Combination cells 150 and 850 have learned to respond to the counter-clockwise direction of rotation



ity cells. Since the ring profile of the presynaptic rotational velocity cells is binary, with each cell signalling that the agent is either rotating in a particular direction (cell fully ring) or is not (cell not ring), the  $w^4$  synaptic weight profiles can be described as a step function of the presynaptic rotational velocity cell ring rate  $r_j^{\text{ROT}}(t)$ . As the four plots display, each postsynaptic combination cell receives positive synaptic weights from the subset of exactly 250 presynaptic rotational velocity cells that signal either clockwise or counter-clockwise rotation (but not both subsets). Combination cells 300 and 1000 have learned to respond to the 250 rotational velocity cells representing clockwise rotation. Combination cells 150 and 850 have learned to respond to the 250 rotational velocity cells representing counter-clockwise rotation. Thus, the postsynaptic combination cells have learned to be maximally stimulated by a particular head direction cell that preferentially stimulates them; but this will only occur if the rotational velocity cells are temporally co-ring with the head direction cells.

The ring rates of the head direction, combination and rotational velocity cells are shown in the plots in Fig. 7. The top left plot displays the ring rates of the head direction cells during the training phase of the experiment. Throughout the training, the activity in the head direction cells is driven by the presence of external visual input. In the time interval 0.0–2.25 s, the agent rotated in a clockwise direction with counter-clockwise rotation occurring in the time interval 2.25–4.5 s. The top right plot displays the ring rates of the head direction cells in the testing phase without external visual input. During the time interval 0.0–1.0 s, there was no ring in the rotational velocity cells (bottom left plot), and a moderate amount of baseline activity in the network of combination cells (bottom right plot); thus, there was a stable packet of head direction cell activity supported by the  $w^1$  recurrent synapses. During the time interval 1.0–2.0 s, the 250 rotational velocity cells representing clockwise rotation became active (bottom left), stimulating activity in the combination cells (bottom right) through the  $w^4$  synapses in conjunction with the head direction cell input through the  $w^3$  synapses. Owing to the high value of the neuronal time constant  $\tau^{\text{COMB}}$  and the asymmetry in the  $w^2$  and  $w^3$

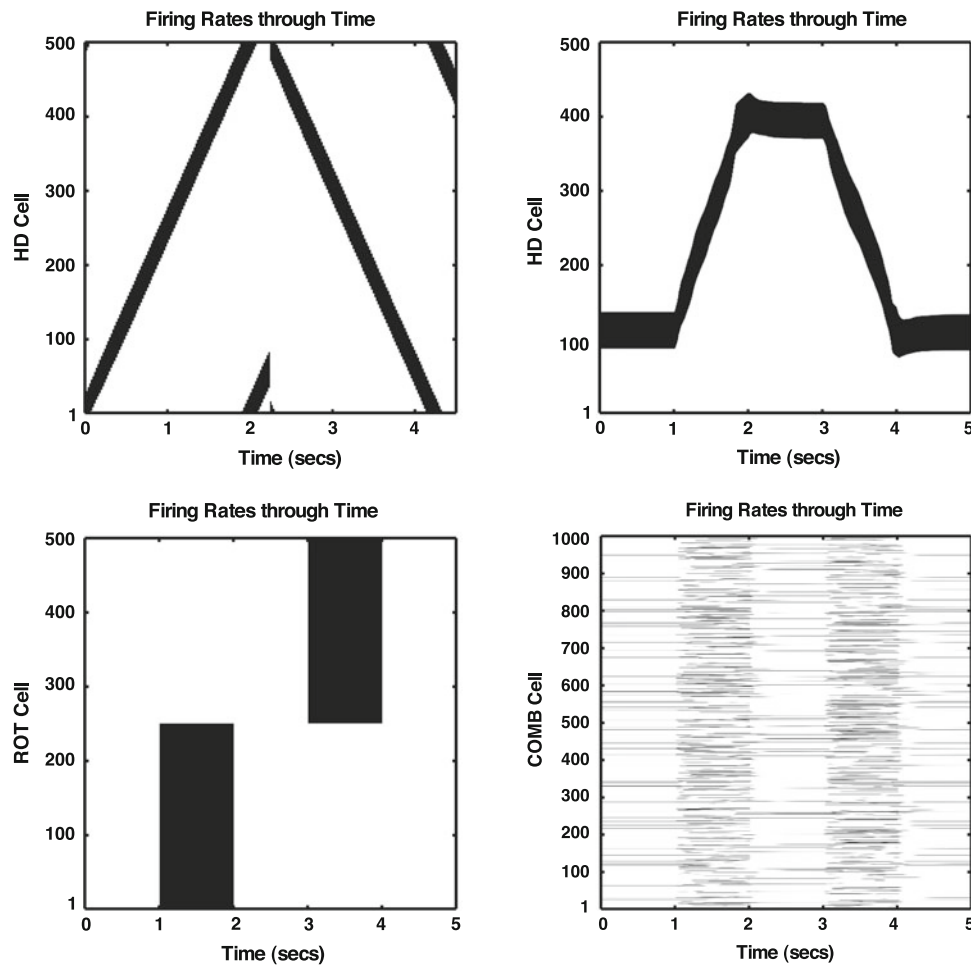


Fig. 7 Firing rates of head direction (HD), combination (COMB), and the packet of HD activity moved through the network in a counter-rotational velocity (ROT) cells during training and testing. These results are taken from a simulation with a time constant of 150 ms, and a rotational velocity of 360°/s (all other parameters are as given in Table 2). *Top left* Firing rates in the network of 500 HD cells during the 4.5 s of training, with the HD cells driven by visual input (0.0–2.25 s: active; 2.25–4.5 s: agent rotating clockwise; 2.25–4.5 s: agent rotating counter-clockwise). *Top right* Firing rates in the network of 500 HD cells during the 5 s of testing in the absence of visual input. During the interval 0.0–1.0 s, the HD cells become active due to the ring of the 250 HD cells. In the interval 1.0–2.0 s, the HD cells become active due to the ring of the 250 HD cells. In the interval 2.0–3.0 s, the HD cells become active due to the ring of the 250 HD cells. In the interval 3.0–4.0 s, the HD cells become active due to the ring of the 250 HD cells. In the interval 4.0–5.0 s, the HD cells become active due to the ring of the 250 HD cells. *Bottom left*: Firing rates in the layer of 500 ROT cells during the 5 s of testing in the absence of visual input. During the interval 1.0–2.0 s, the ROT cells representing clockwise rotation are active. During the interval 3.0–4.0 s, the ROT cells representing counter-clockwise rotation are active. *Bottom right* Firing rates in the network of 1000 COMB cells during the 5 s of testing in the absence of visual input. In the interval 1.0–2.0 s, the COMB cells become active due to the ring of the 250 HD cells. In the interval 3.0–4.0 s, the COMB cells become active due to the ring of the 250 HD cells. In all plots, regions of high activity are represented by darker shading.

synaptic weight profiles produced during learning, the amount of baseline activity in the combination cells; thus, during this period of the test phase stimulated head direction cells representing head direction cell network. During the time interval 3.0–4.0 s, the 250 rotational velocity cells representing counter-clockwise rotation started firing (bottom left), in turn, stimulating activity in the combination cell network (bottom right). In an identical mechanism to that for clockwise rotation, the model thus performed velocity path integration of head direction, but this time in the counter-clockwise direction

Table 3 Speed of movement of the head direction activity packet during testing in the absence of visual input

	Clockwise	Counter-clockwise
$\tau^{\text{COMB}}$ 150 ms; 360/s Rotational velocity		
Mean speed	180°/s	2017°/s
Standard error	10°/s	80°/s
Percentage	50%	560%
$\tau^{\text{COMB}}$ 150 ms; 180/s Rotational velocity		
Mean speed	125°/s	1255°/s
Standard error	9°/s	7.5°/s
Percentage	69%	697%
$\tau^{\text{COMB}}$ 100 ms; 360/s Rotational velocity		
Mean speed	208°/s	2241°/s
Standard error	15°/s	32°/s
Percentage	58%	623%
$\tau^{\text{COMB}}$ 100 ms; 180/s Rotational velocity		
Mean speed	112°/s	1042°/s
Standard error	5°/s	4.3°/s
Percentage	65%	57.9%

For all of the four experiments, the results are computed over six simulation runs. Within an experiment, each of the six simulations had identical model parameters but different random synaptic connectivity and different random synaptic weight initializations. The table displays the mean speed of the activity packet across the six simulations during testing as calculated according to Eq. 19; the standard error of the mean; and the mean speed of the activity packet as a percentage of the speed of rotation of the agent that was imposed during training in the presence of visual input. For each experiment, results are displayed for both clockwise and counter-clockwise rotations of the activity packet during testing

of rotation. During the time interval 4.0–5.0 s, the rotational velocity cells started ring velocity cells ceased ring, the activity level in the combination cell network returned to a baseline level and again to the high value of the neuronal time constant  $\tau^{\text{COMB}}$ , and there was a stable packet of activity in the head direction cell network. (The head direction cell activity packet through the head direction cell network.)

In order to determine whether the model could perform velocity path integration of head direction at the same speed during testing as was imposed during training, the speed of update of the head direction cell activity packet was recorded. The measurement was taken according to

$$\text{speed} = \left| \frac{p_2 - p_1}{t_2 - t_1} \right| \tag{18}$$

where  $p_1$  and  $p_2$  represent the start and end positions respectively (in degrees) of the packet of head direction cell activity; and  $t_1$  and  $t_2$  represent the time (in s) at which the start and end packet positions were obtained. The packet positions were calculated as follows:

$$p = \frac{\sum_i r_i \theta_i}{\sum_i r_i} \tag{19}$$

where  $r_i$  is the firing rate of postsynaptic head direction cell  $i$ , and  $\theta_i$  is the preferred head direction for postsynaptic head direction cell  $i$  in the presence of visual input.

Measurements of speed were taken for 0.5 s during both the clockwise (1.25–1.75 s) and counter-clockwise (3.25–3.75 s) periods of rotation during testing. (The recording was

Six simulations were conducted, and in each simulation the same model parameters were employed, with the exception of different random synaptic connectivity and different random synaptic weight initialization. Table 3 summarizes the statistics we carried out on the results. The mean speed of rotation across the six simulations was 180°/s for clockwise rotation, and 2017°/s for counter-clockwise rotation. This is compared to a true speed of 360°/s during training in the presence of external visual input. Standard errors of 19.4°/s for clockwise rotation, and 8°/s for counter-clockwise rotation indicate a small amount of variation across the six simulations, but the standard errors are still sufficiently small to conclude that the simulations produced speeds of rotation consistent enough with one another to produce reliable results. In order to further compare the recorded speed during testing to the speed imposed during training, the mean speed was calculated during testing as a percentage of the speed during training. For the period of clockwise rotation, the model updated the packet of head direction cell activity at a speed that was 50% of that imposed during training. For the period of counter-clockwise rotation, the speed was 56.0% of the speed during training. The model has learned

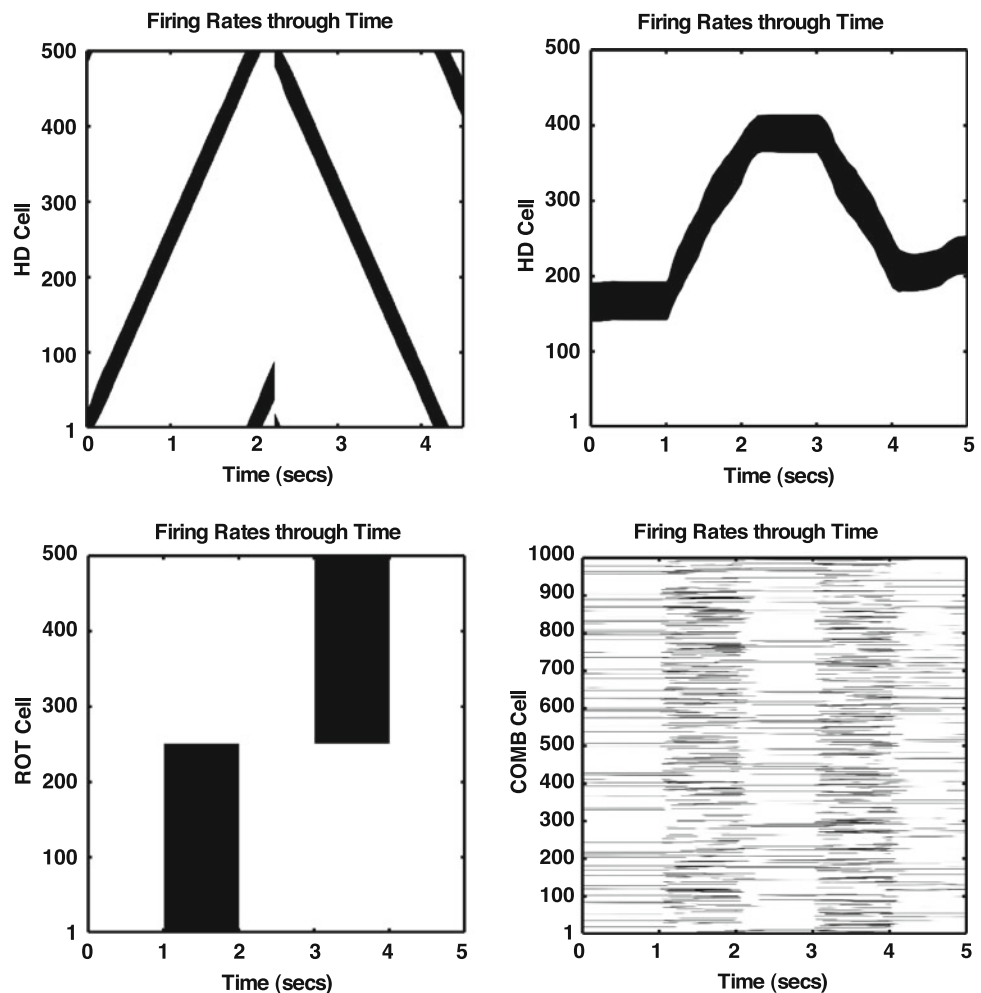
to achieve this automatically without the need to carefully hand-tune a parameter specifically governing the speed at which the model was used by [Stringer and Rolls \(2006\)](#). We note, however, that while the speed at testing is a reasonable approximation (and for Fig. 7, and so is the interpretation. When the same model is within the same order of magnitude) of the speed imposed during training, the speeds during testing are regularly below those during training. In future study, we will investigate what architectural features contribute to this underestimation of the speed during path integration.

### 3.2 Experiment 2 $\tau^{COMB} = 150\text{ ms}$ ; $180^\circ/\text{s}$ rotational velocity

We conducted this experiment to demonstrate that if the model was trained with the same parameter set but at half the rotational velocity compared to Experiment 1, then during the testing phase the model would still perform path integration at the correct speed. Thus, the same model can learn and perform path integration at different rotational velocities. Except for the difference in head direction cells, and the rotational velocity, all the model parameters were the same as for Experiment 1 (as given in [Table 2](#)).

The plots in [Fig 8](#) display the firing rates of the head direction (HD), combination, and rotational velocity cells during training and testing of the model. The conventions are the same as in [Fig. 7](#), and so is the interpretation. When the same model is trained at half the rotational velocity compared to Experiment 1, the same mechanism of a high value for the neuronal time constant  $\tau^{COMB}$  on the activations of the combination cells produces a natural time delay between the activity profile in the head direction cell network and the activity profile in the combination cell network. During this delay, the head direction of the agent will have changed. Thus, at any given moment in time, the most active combination cell learns to preferentially stimulate the head direction cell representing the new head direction. This learned association will help to shift a packet of head direction cell activity through the head direction cell network. Much similar to Experiment 1, the current model also requires temporally conjunctive inputs to the combination cells through the  $3^{\text{rd}}$  synapses from the different head direction cells, and the  $4^{\text{th}}$  synapses from the rotational velocity cells, in order for the combination cells to start firing and, in turn, stimulate an activity packet in the head direction

Fig. 8 Firing rates of head direction (HD), combination (COMB) and rotational velocity (ROT) cells during training and testing. These results are taken from a simulation with a time constant  $\tau^{COMB}$  of 150 ms, and a rotational velocity of  $180^\circ/\text{s}$  (all other parameters are as given in [Table 2](#)). Conventions are as for [Fig 7](#)



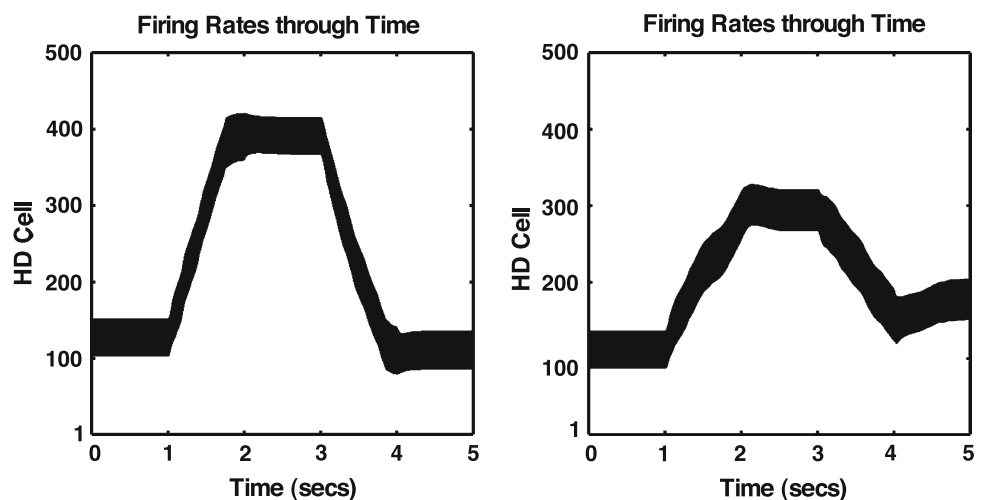


cell network (bottom left and right plots). When there is no but regular underestimation. Moreover, the same model with ring in the layer of rotational velocity cells, there is only a the same set of parameters is able to learn two completely moderate amount of baseline activity in the combination cell different rotational velocities during training, and reproduce network, and, thus, there is a stable packet of activity in the (within a small margin of error) those velocities during the head direction cell network (top right plot). testing phase.

In order to determine whether the model had learned to update the packet of head direction cell activity at the same speed during testing as was imposed during training, we measured the speed of the update according to 18qs. This experiment was conducted to demonstrate that the same and 19. We took measurements across a 0.5 s interval for both clockwise and counter-clockwise rotation, and repeated these measurements across six different simulations that had identical model parameters with the exception of different random synaptic connectivity and different random synaptic weight initialization. The results we obtained are summarized in Table 3.

The mean speed of rotation was 125/s for the period of clockwise rotation, and 125/s for the period of counter-clockwise rotation. This is compared to the true speed during training of 180°/s. Standard errors of 9/s for the clockwise measurements and 57/s for the counter-clockwise measurements, indicate a small degree of variability across the six simulations, but the standard errors are small enough to conclude that the simulations produced speeds of rotation consistent enough with one another to be considered as reliable results. We also calculated the mean speed of the activity packet during testing as a percentage of the rotational velocity imposed during training. For the period of clockwise rotation, the mean speed during testing was 69.5% of the rotational velocity imposed during training. For the period of counter-clockwise rotation, the mean speed was 697% of the rotational velocity imposed during training. Similar to Experiment 1, the speeds recorded during testing of the model are a reasonable approximation to those experienced during training of the model, although there is a small

Fig. 9 Firing rates of head direction (HD) cells during testing. These results are taken from simulations with a time constant  $t^{COMB}$  of 100 ms and rotational velocities during training of 360°/s (Left plot) and 180°/s (Right plot). Conventions are as for the top-right plots in Figs. 7 and 8





be a different cell to the one which preferentially stimulates the values of the neuronal time constants for the head direction cell. Essentially, the model learns to make combination cells. In these simulations, we found that the accuracy of path integration during testing was significantly degraded by having larger values for the neuronal time constants for the head direction cells. Thus, we observed an asymmetry between the effects of the neuronal time constants for the combination cells and the head direction cells. The path integration mechanism described in this paper was successful only over the effective delays in neurotransmission from the head direction cells to the combination cells due to large delays in neurotransmission from the combination cells to the head direction cells due to large delays.

In the four experiments we conducted, the model did not reproduce the exact speed during testing that was imposed during training. This could be due to the fact that our simulated models were relatively small, containing only 2000 neurons in total. This small architecture may be more susceptible to noise in the system due to an inability to average the noise out as well as a larger architecture, and the noise may lead to the packet of head direction cell activity updating at a slower speed than the model was trained with. A model with a larger architecture may, thus, show less difference between the speeds recorded during testing and those imposed during training, when compared to the results we presented in this article. Unfortunately, owing to the large simulation run-time, we were unable to investigate the performance in a larger network in this study. We hope to examine this issue further in future research.

We know of no previous model that can update a packet of head direction cell activity at the correct speed through self-organization with biologically plausible learning rules. Hahnloser (2003) used an error correction learning rule in a network with separate head direction subnetworks for each direction of idiothetic signal to produce a direction of the agent. The only way to ameliorate this inaccuracy is to implement a relatively small neuronal time constant for the head direction cells. Alternatively, we hypothesize that one way in which the path integration accuracy of the model might be improved is by introducing explicit time delays into the learning rules for the  $w^2$  and  $w^3$  synaptic weights,

In order for the current model to operate correctly for different rotational velocities, it is necessary to have different rotational velocity cells tuned to those different velocities. This has already been investigated by Walters et al. (2009). These authors have simulated path integration in a similar network architecture with axonal transmission delays incorporated into the equations governing both the cell activations and the corresponding learning rules. These authors have reported more accurate path integration during testing. We have shown in this article that the model can, without the need to alter any model parameters, learn to perform path integration when trained with different rotational velocities, and it would be interesting to confirm that in the value of the time constant the same model can be trained on different rotational velocities at the same time. Training with just a few velocities should suffice to allow the model to generalize over a range of velocities. We chose to vary the neuronal time constant across the experiments conducted, whilst keeping the neuronal time constant constant, to clarify the principle that an increase in the value of the time constant is approximately proportional to an increase in the effective natural time delay. Thus, the same model can learn to perform path integration when implemented with different time delays. Moreover, the analytical argument given in Sect. 1 should apply to any

In the simulations of the two-layer network described above, the neuronal time constants implemented for combination cell  $\rightarrow$  head direction cell over a broad range of possible neuronal time constants. Further, individual three-cell circuits should be able to operate in parallel with other three-cell circuits with different time constants, i.e. where

$\tau^{\text{HD}}$ ,  $\tau^{\text{COMB}}$  and  $\tau^{\text{HD}}$  for the three cells are set to different values. Therefore, we hypothesise that the model should still self-organize and perform path integration at the correct speed if the neuronal time constants  $\tau^{\text{HD}}$  and  $\tau^{\text{COMB}}$  for individual head direction and combination cells were drawn from a distribution of time constants, instead of being homogeneous for each cell type. We plan to test this hypothesis in future simulations.

In the models simulated, we used values of 100 and 150 ms for the neuronal time constant  $\tau^{\text{COMB}}$ , and a constant value of 1 ms across all simulations for the neuronal time constant  $\tau^{\text{HD}}$ . A possible way in which the different time constants—the key principle of operation for the current model—could be implemented in the brain is through the use of AMPA receptor-mediated synaptic transmission for faster time constants (in the case of the current model, this would be the head direction cells), and NMDA receptor-mediated synaptic transmission for slower time constants (the combination cells in the current model). The time constant for AMPA currents is approximately 2 ms, while the time constant for NMDA currents is approximately 100–150 ms (Srinivasan et al. 1990; Spruston et al. 1995; Brunel and Wang 2001). Thus, the values we have implemented are within the range of biological plausibility.

One of the key components of the current model is the presence of combination cells that learn to respond to combinations of a particular head direction and a rotational velocity. For the proposed architecture to be implemented in the brain, there would, thus, need to be classes of neurons that respond to combinations of spatial information and velocity. Previous research has revealed that there are neurons that respond to a combination of head direction and angular rotation velocity (Taube et al. 1990; Sharp 1996; Bassett and Taube 2005). It has also been shown that hippocampal place cells can have their activity modulated by running speed (McNaughton et al. 1983), and can even be tuned to particular velocities (Saksner et al. 1989). The current theory provides an account of the presence of such cells in the hippocampus. The origin of these signals, and indeed a possible brain region for path integration of place to be implemented, is the dorsocaudal medial entorhinal cortex which contains spatial grid cells that are modulated by head direction and forward velocity (Hafting et al. 2005; Sargolini et al. 2006).

Finally, we suggest that path integration implemented in the way described in this article could be performed in other brain systems, including the hippocampal place cell system (O'Keefe and Dostrovsky 1971; McNaughton et al. 1983; Muller et al. 1991) and the hippocampal spatial view system of neurons that respond when a primate looks at a particular location in space, which are updated by idiothetic eye movements made in the dark (Robertson et al. 1998, 1999; Rolls 1999; Rolls and Xiang 2006).

**Acknowledgement** This research was supported by the Economic and Social Research Council and the Wellcome Trust.

## References

- Amari S (1977) Dynamics of pattern formation in lateral-inhibition type neural elds. *Biol Cybern* 27:77–87
- Bassett J, Taube JS (2005) Head direction signal generation: ascending and descending information streams. In: Wiener SI, Taube JS (eds) *Head direction cells and the neural mechanisms of Spatial orientation*, pp 83–109. MIT Press, Cambridge
- Brunel N, Wang X-J (2001) Effects of neuromodulation in a cortical network model of object working memory dominated by recurrent inhibition. *J Comput Neurosci* 11:63–85
- Collett TS, Zeil J (1998) Places and landmarks: an arthropod perspective. In: Healy S (ed) *Spatial representation in animals*. Oxford University Press, Oxford
- Georges-François P, Rolls ET, Robertson RG (1999) Spatial view cells in the primate hippocampus: allocentric view not head direction or eye position or place. *Cereb Cortex* 9:197–212
- Hafting T, Fyhn M, Molden S, Moser MB, Moser EI (2005) Microstructure of a spatial map in the entorhinal cortex. *Nature* 436:801–806
- Hahnloser RHR (2003) Emergence of neural integration in the head-direction system by visual supervision. *Neuroscience* 120:877–891
- Hestrin S, Sah P, Nicoll R (1990) Mechanisms generating the time course of dual component excitatory synaptic currents recorded in hippocampal slices. *Neuron* 5:247–253
- McNaughton BL, Barnes CA, O'Keefe J (1983) The contributions of position, direction, and velocity to single unit activity in the hippocampus of freely-moving rats. *Exp Brain Res* 52:41–49
- Mittelstaedt H, Mittelstaedt ML (1982) Homing by path integration. In: Papi F, Wallraff HG (eds), *Avian navigation*, pp 290–297. Springer, Berlin
- Mittelstaedt ML, Mittelstaedt H (1980) Homing by path integration in a mammal. *Naturwissenschaften* 67:566–567
- Muller RU, Kubie JL, Bostock EM, Taube JS, Quirk GJ (1991) Spatial ring correlates of neurons in the hippocampal formation of freely moving rats. In: Paillard J (ed) *Brain and space*, pp 296–333. Oxford University Press, Oxford
- Muller RU, Ranck JB Jr, Taube JS (1996) Head direction cells: properties and functional significance. *Curr Opin Neurobiol* 6:196–206
- Oja E (1982) A simplified neuron model as a principal component analyzer. *J Math Biol* 15:267–273
- O'Keefe J, Dostrovsky J (1971) The hippocampus as a spatial map: preliminary evidence from unit activity in the freely moving rat. *Brain Res* 34:171–175
- Ranck JB Jr (1985) Head direction cells in the deep cell layer of dorsolateral presubiculum in freely moving rats. In: Buzsáki G, Vanderwolf CH (eds) *Electrical activity of the archicortex*. Akadémiai Kiadó, Budapest
- Redish AD (1999) *Beyond the cognitive map*. MIT Press, Cambridge
- Redish AD, Elga AN, Touretzky DS (1996) A coupled attractor model of the rodent head direction system. *Netw Comput Neural Syst* 7:671–685
- Robertson RG, Rolls ET, Georges-François P (1998) Spatial view cells in the primate hippocampus: effects of removal of view details. *J Neurophysiol* 79:1145–1156
- Robertson RG, Rolls ET, Georges-François P (1999) Head direction cells in the primate pre-subiculum. *Hippocampus* 9:206–219
- Rolls ET, Treves A (1998) *Neural networks and brain function*. Oxford University Press, Oxford

- Rolls ET (1999) Spatial view cells and the representation of place in the primate hippocampus. *Hippocampus* 9:467–480
- Rolls ET, Xiang JZ (2006) Spatial view cells in the primate hippocampus, and memory recall. *Rev Neurosci* 17:175–200
- Rolls ET, Robertson RG, Georges-François P (1997) Spatial view cells in the primate hippocampus. *Eur J Neurosci* 9:1789–1794
- Samsonovich A, McNaughton BL (1997) Path integration and cognitive mapping in a continuous attractor neural network model. *J Neurosci* 17:5900–5920
- Sargolini F, Fyhn M, Hafting T, McNaughton BL, Witter MP, Moser MB, Moser EI (2006) Conjunctive representation of position, direction, and velocity in entorhinal cortex. *Science* 312:758–762
- Sharp PE (1996) Multiple spatial-behavioral correlates for cells in the rat postsubiculum: multiple regression analysis and comparison to other hippocampal areas. *Cereb Cortex* 6:238–259
- Skaggs WE, Knierim JJ, Kudrimoti HS, McNaughton BL (1995) A model of the neural basis of the rat's sense of direction. In: Tesau-ro G, Touretzky DS, Leen TK (eds) *Advances in neural information processing Systems*, vol 7, pp 173–180. MIT Press, Cambridge
- Song P, Wang X-J (2005) Angular path integration by moving “hill of activity”: a spiking neuron model without recurrent excitation of the head-direction system. *J Neurosci* 25:1002–1014
- Spruston N, Jonas P, Sakmann B (1995) Dendrite glutamate receptor channels in rat hippocampal CA3 and CA1 pyramidal neurons. *J Physiol* 482:325–352
- Stringer SM, Rolls ET (2006) Self-organizing path integration using a linked continuous attractor and competitive network: path integration of head direction. *Netw Comput Neural Syst* 17:419–445
- Stringer SM, Trappenberg TP, Rolls ET, De Araujo IET (2002) Self-organizing continuous attractor networks and path integration: One dimensional models of head direction cells. *Netw Comput Neural Syst* 13:217–242
- Taube JS, Muller RU, Ranck JB Jr (1990a) Head-direction cells recorded from the postsubiculum in freely moving rats. I. Description and quantitative analysis. *J Neurosci* 10:436–447
- Taube JS, Muller RU, Ranck JB Jr (1990b) Head-direction cells recorded from the postsubiculum in freely moving rats. II. Effects of environmental manipulations. *J Neurosci* 10:436–447
- Taylor JG (1999) Neural ‘bubble’ dynamics in two dimensions: foundations. *Biol Cybern* 80:393–409
- Walters DM, Stringer SM, Rolls ET (2009) Path integration of head direction: updating a packet of neural activity at the correct speed using axonal conduction delays (submitted)
- Wiener SI, Paul CA, Eichenbaum H (1989) Spatial and behavioural correlates of neuronal activity. *J Neurosci* 9:2737–2763
- Zhang K (1996) Representation of spatial orientation by the intrinsic dynamics of the head-direction cell ensemble: a theory. *J Neurosci* 16:2112–2126